Development of a surface shape for the heat transfer enhancement and reduction of pressure loss in an internal cooling passage

Jeong Hoon Doo
School of Mechanical Engineering,
Pusan National University
Busan, 609-735, Korea
djh219@pusan.ac.kr

Hyun Sik Yoon
Advanced Ship Engineering Research Center,
Pusan National University
Busan, 609-735, Korea
lesmodel@pusan.ac.kr

Man Yeong Ha
School of Mechanical Engineering,
Pusan National University
Busan, 609-735, Korea
myha@pusan.ac.kr

ABSTRACT

A new surface shape of an internal cooling passage which largely reduces the pressure drop and enhances the surface heat transfer is proposed in the present study. The Riblet-mounted Dimple as the new surface shape is consisted of the concave dimple and the riblet which is protruded along the streamwise direction. Direct numerical simulations were conducted in order to simulate the fully developed turbulent flow and thermal fields through the cooling passage at the Reynolds number of 2,800 based on the mean bulk velocity and channel height and Prandtl number of 0.71 (air). The mean pressure gradient is calculated in order to keep the mass flow rate constant in the streamwise direction. The thermo-aerodynamic performance for five different cases considered in the present study was assessed in terms of the Nusselt number, Stanton number, Fanning friction factor, volume goodness factor and area goodness factor. At the riblet angle of $60°$ among the riblet angles considered in this study, the drag reduced about -22.86% and Nusselt number augmented about 7.05%.

INTRODUCTION

Both the drag reduction and heat transfer enhancement in an internal cooling passage are required in order to improve the durability and efficiency of many practical applications with internal cooling passages such as combustion chamber liners, internal cooling passages of turbine airfoils in gas turbine engines, heat exchangers and many other applications. Thus, in order to meet these requirements, many researchers have developed the advanced heat transfer augmentators such as rib turbulators, arrays of pin fins and arrays of dimples to apply the internal cooling passages. Among these devices, the arrays of dimples enhance the heat transfer augmentation with lower pressure drop in comparison with other types of heat transfer augmentator. Consequently, many researches have been conducted in order to reveal the flow structure and heat transfer enhancement mechanisms which are caused by the dimple-mounted surface in the flow passage. The representative researches for the dimple are as follows.

Afanasyev et al. (1993) calculated the overall heat transfer and pressure drop for the passage with the dimple-mounted surface ($\delta/D = 0.067$) in the turbulent flow regime and reported the heat transfer augmentation of $30\sim40\%$ with the negligible pressure drop. Moon et al. (2000) experimentally measured heat transfer coefficients and friction factors for a variation of a ratio of channel height to dimple diameter in rectangular channels which had dimples on one wall in a Reynolds number range from 12000 to 60000. They reported that the variation of the ratio is almost independent of the heat transfer augmentation on the dimpled wall which had 2.1 times that of smooth channel. Ligrani et al. (2001) studied the time-varying dynamic flow pattern and time-averaged flow structure for a dimpled surface in a channel using flow visualization techniques in a Reynolds number range from 600 to 11000 with three different channel heights. They presented the existence of a primary vortex pair formed at the central portion of a dimple and two secondary vortex pairs formed near the spanwise edges of a dimple. And they observed that a primary vortex is periodically shed from the central portion of each dimple. They reported that the strength of the secondary flow structures increases as the channel height decreases. Mahmood and Ligrani (2002) carried out the experimental study to investigate combined influences of a variation of channel height, ratio of air inlet

Sixth International Symposium on Turbulence and Shear Flow Phenomena
Seoul, Korea, 22-24 June 2009

Table 1: Design variables used in the present study

CASE No	θ	d	h_R	δ	S
1	0°	2	0	0.40	0
2	15°	2	0.39	0.39	0.21
3	30°	2	0.38	0.38	0.44
4	45°	2	0.36	0.36	0.71
5	60°	2	0.30	0.30	1.05

stagnation temperature to surface temperature and Reynolds number in a channel with a dimpled surface. The results based the experimental measurement were revealed that local Nusselt number augmentations increases at the same locations as decreases both the channel height and the ratio of the air inlet stagnation temperature to the surface temperature. Other researchers also have conducted their studies to find out the characteristics of the flow structure and heat transfer in the flow passage with the dimple-mounted surface. Even the dimple shape gives less the pressure drop than the other types of devices, still the existence of the pressure drop in nature is the main source to induce the lower thermo-aerodynamic performance in the flow passage.

Therefore, the main purpose of the present study is to develop a new surface shape to improve the thermo-aerodynamic performance in terms of the increase of Nusselt number and the decrease of the pressure drop. Subsequently, the enhancement mechanisms of the thermo-aerodynamic performance are studied by carefully analyzing the flow and thermal structures. Also, the quantity information as the characteristics of flow and thermal fields such as the Nusselt number, Stanton number, Fanning friction factor, volume goodness factor and area goodness factor has been presented in detail.

NUMERICAL METHOD

Governing equation

The governing equations describing the three-dimensional unsteady incompressible viscous flow and thermal fields are the continuity, momentum and energy equations.

$$\nabla \cdot \mathbf{u} = 0 \tag{1}$$

$$\frac{\partial \mathbf{u}}{\partial t} + (\mathbf{u} \cdot \nabla)\mathbf{u} = -\nabla p + \frac{1}{\text{Re}}\nabla^2 \mathbf{u} + \mathbf{\Pi} \tag{2}$$

$$\frac{\partial T}{\partial t} + \mathbf{u} \cdot \nabla T = \frac{1}{\text{Re Pr}}\nabla^2 T \tag{3}$$

The variables in the above equations are normalized by the channel height H and mean bulk velocity u_m. The normalization results in two dimensionless parameters as bellows.

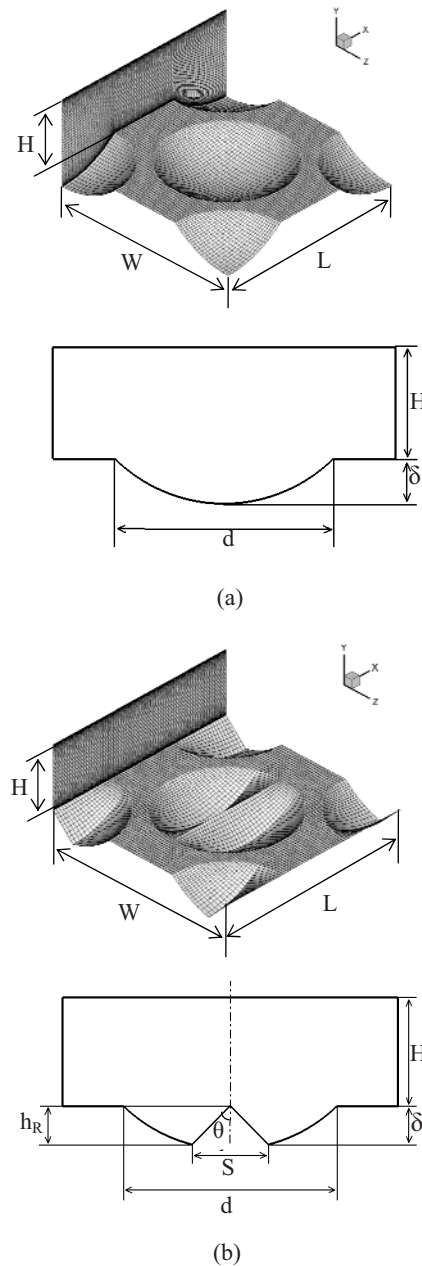$$\text{Re}_m = \frac{u_m H}{\nu} \, , \, \text{Pr} = \frac{\nu}{\alpha} \tag{4}$$

(a)

(b)

Figure 1: Configurations and grid distribution of; (a) General Dimple, (b) Riblet-mounted Dimple

In the above equations, ν and α represent the kinematic viscosity and thermal diffusivity, respectively.

In order to keep the mass flow rate constant in time, a technique proposed by You et al. (2000) is used in the present study. In Eq. (2), the mean pressure gradient $\mathbf{\Pi}$ of the streamwise direction is calculated at each time step and the momentum loss in the control volume is compensated by the mean pressure gradient $\mathbf{\Pi}$.

A central difference scheme with second-order accuracy based on the finite volume method is used for the spatial discretization. A two-step time-split scheme is used in order to advance the flow field and the continuity is satisfied through the solution of the Poisson equation. In the

Table 2: Validation results of our CFD code

		f_D
Flat channel $\mathrm{Re}_m = 5600$	Present study	8.13×10^{-3}
	Kim et al. (1987)	8.18×10^{-3}
Dimpled channel $\mathrm{Re}_m = 3900$	Present study	1.74×10^{-2}
	Wang et al. (2006)	1.75×10^{-2}

Table 3: Ratios of drag reduction and Nusselt number augmentation

CASE No	θ	ΔD [%]	ΔNu [%]
2	15°	−3.16	−0.54
3	30°	−6.51	−2.28
4	45°	−9.48	4.66
5	60°	−22.86	7.05

momentum and energy equations, the nonlinear terms are treated explicitly using the second-order Adams-Bashforth scheme and the diffusion terms are treated implicitly using the second-order Crank-Nicolson scheme.

In Fig. 1, x, y and z directions represent the streamwise, wall-normal and spanwise directions, respectively. For the flow and thermal boundary conditions, the no-slip and constant temperature conditions are imposed at the upper and lower walls and periodic conditions are imposed in the x and z directions, respectively.

Computational domain and Grid resolution

The shape of the General Dimple used in the previous researches and the shape of the Riblet-mounted Dimple as the new surface shape proposed in the present study are shown in Figs. 1(a) and 1(b), respectively, where θ, d, S, h_R and δ represent the riblet angle, dimple-imprinted diameter, riblet spacing, riblet height and dimple-imprinted depth, respectively. In this study, the dimension of h_R is kept to be identical to that of δ in the case of the Riblet-mounted Dimple shape. As shown in Fig. 1(b), the Riblet-mounted Dimple is consisted of the concave dimple and the riblet which is protruded along the streamwise direction.

The present study considers five cases including one General Dimple shape and four different Riblet-mounted Dimple shapes. The design variables and size of the computational domain used in the present study are summarized in table 1. In case of the General Dimple, even the design variables of θ, h_R and S related to riblet are not defined, those are given the values as $0°$, 0 and 0 in order to unify the denotation, respectively. It is very important to choose the suitable size of the computational domain with the periodicity-imposed boundary regions in order to minimize the computational cost and be capable of obtaining all the information of the relevant physical phenomena in the numerical solution. In the present study, the size of the computational domain was selected on the basis of the previous research which was conducted by Elyyan et al. (2008). Therefore, the size of the computational domain used in the present study has $\pi \times 1 \times \pi$ in the x, y, z directions, respectively. The grid points of $65 \times 65 \times 81$ were distributed in the x, y and z directions, respectively. The location of the first grid point away from the wall in the wall-normal direction is $y^+ \approx 0.6$ as wall units($^+$) and the mean spacings of the grid points

distributed in the x, z directions are $\Delta x^+ \approx 10$ and $\Delta z^+ \approx 8$, respectively.

Direct numerical simulations were conducted for the flat channel flow at $\mathrm{Re}_m = 5600$ and dimpled channel flow at $\mathrm{Re}_m = 3900$ in order to verify the accuracy of the present numerical methods. Representatively, Darcy friction factors f_D have been considered as defined following;

$$f_D = \frac{2H\Delta P}{\rho u^2 L} \tag{5}$$

In conclusion, the present results are very good agreement with those of the previous researches as shown in Table 2.

RESULTS

Thermo-aerodynamic performance

Table 3 shows the ratios of drag reduction ΔD and Nusselt number augmentation ΔNu which are defined as below, respectively.

$$\Delta D = \frac{\langle \overline{D} \rangle - \langle \overline{D_0} \rangle}{\langle \overline{D_0} \rangle} \times 100 \tag{6}$$

$$\Delta Nu = \frac{\langle \overline{Nu} \rangle - \langle \overline{Nu_0} \rangle}{\langle \overline{Nu_0} \rangle} \times 100 \tag{7}$$

where, $\langle \overline{D_0} \rangle$ and $\langle \overline{D} \rangle$ represent the time- and surface-averaged total drag of CASE1 (General Dimple) and CASE2~CASE5 (Riblet-mounted Dimple), respectively and $\langle \overline{Nu_0} \rangle$ and $\langle \overline{Nu} \rangle$ represent the time- and surface-averaged Nusselt number of CASE1 and CASE2~CASE5, respectively.

Regardless of the riblet angle for the Riblet-mounted Dimple, the value of drag reduction ratio reveals the negative value, meaning that the drag is decreased in the comparison with that of the General dimple. The drag reduction ratio augments with increasing the riblet angle. As a result, at $\theta = 60°$, drag reduction ratio reaches to about -22.86%.
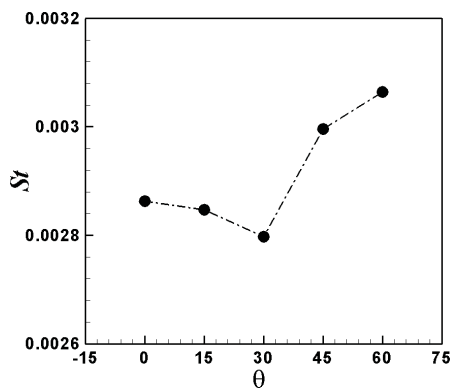
In contrast to the drag reduction ratio, the ratio of Nusselt number augmentation has the deflection point in between 30° and 45°. Thus, with increasing θ from 0° to
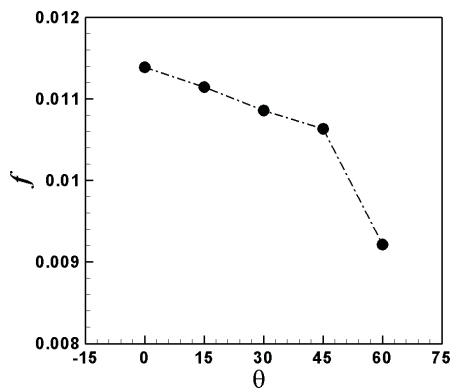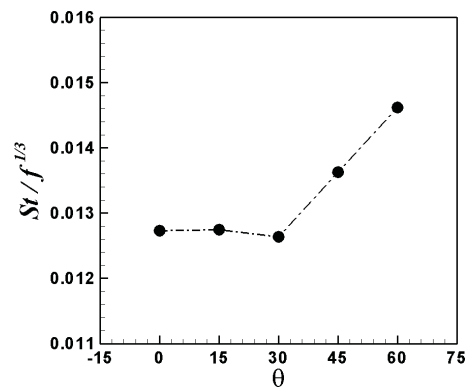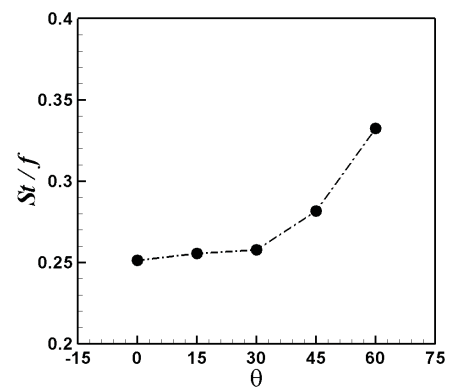
Figure 2: Distribution of the quantities as a function of θ;
(a) Fanning friction factor, (b) Stanton number

Figure 3: Distribution of the quantities as a function of θ;
(a) volume goodness factor, (b) area goodness factor

$30°$, the ratio of Nusselt number augmentation increases with the negative value. Further θ increases to $45°$, the ratio of Nusselt number augmentation reveals the positive value which means the enhancement of the heat transfer. When θ incrase from $45°$ to $60°$, the ratio of Nusselt number augmentation keeps increasing in magnitude as the positive value.

Figs. 2(a) and 2(b) show the distribution of the Fanning friction factor and Stanton number as a function of θ, respectively. Fanning friction factor and Stanton number were calculated in order to assess the quantitative pressure drop and heat transfer performances for the different heat transfer surfaces, respectively. Fanning friction factor f and Stanton number St are defined as below, respectively.

$$f = \frac{H\Delta P}{2\rho U_m^2 L} \quad (8)$$

$$St = \frac{Nu}{Re\,Pr} \quad (9)$$

The Fanning friction factor linearly decreases as θ increases from $0°$ to $45°$ and rapidly decreases at $\theta = 60°$ as shown in Fig. 2(a). Consequently, it is clear that the pressure drop is reduced by the installation of the riblet

inside dimple. The Stanton number gradually decreases as θ increases from $0°$ to $30°$.

However, the Stanton number steeply increases as θ increases from $30°$ to $60°$ and enventually has the maximum value at $\theta = 60°$, which is consistent with the variation of the the ratio of Nusselt number augmentation as explained in Table 3.

The volume goodness factor and area goodness factor proposed by Shah and London (1978) are calculated in order to evaluate the quantitative thermo-aerodynamic performance for the different heat transfer surfaces and these factors are defined as follows, respectively.

$$\text{Volume goodness factor} = \frac{St}{f^{1/3}} \quad (11)$$

$$\text{Area goodness factor} = \frac{St}{f} \quad (12)$$

The higher volume goodness factor is required the smaller heat trasnfer surface area. Consequently, the smaller volume of heat exchanger matrix is required. The higher area goodness factor is required the smaller frontal area of the heat exchanger matrix. Figs. 3(a) and 3(b) show the distribution of the volume goodness factor and area
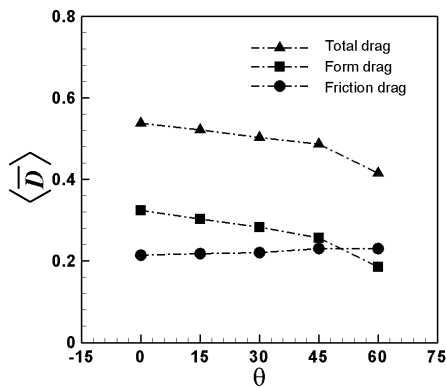
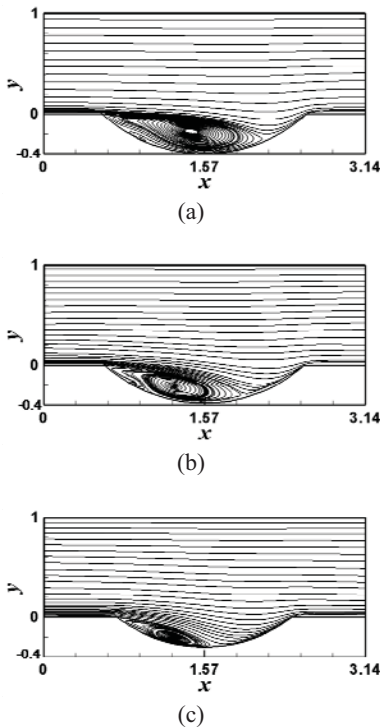Figure 4: Distribution of the time- and surface-averaged drag as a function of θ

(a)

(b)

(c)

Figure 5: Time-averaged streamlines in the spanwise-normal plane at the Base line; (a) CASE1, (b) CASE3, (c) CASE5
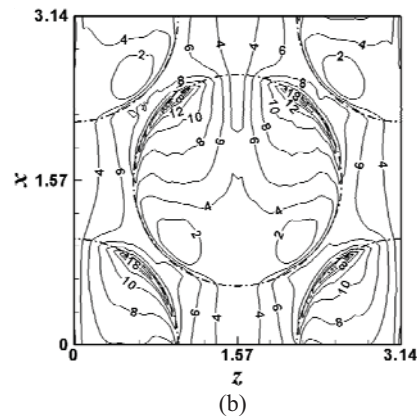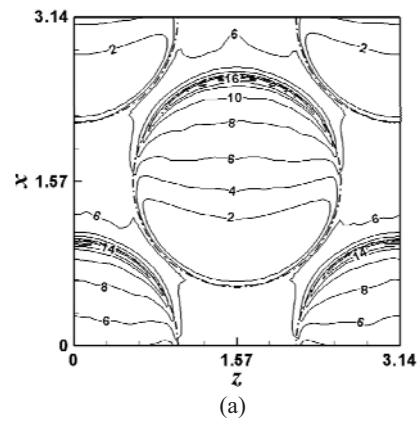

(a)

(b)

Figure 6: Distribution of the time-averaged local Nusselt number at the bottom surface; (a) CASE1, (b) CASE5

Fig. 4 shows the distribution of the time- and surface-averaged form, friction and total drags as a function of θ. The form drag gradually decreases with increasing θ from $0°$ to $45°$ and rapidly decreases with continuatally increasing to $\theta = 60°$. As well known, the form drag is mainly caused by the concave surface located in the downstream portion inside the dimple. When the riblet is installed into the dimple, the concave surface is gradually flattened out as θ increases. Thus, flow resistance is weak, which leads to the form drag reduction. However, the friction drag linearly grows with increasing θ. Because the form drag is dominant to the friction drag, the variation of the total drag follows the pattern of the form drag according to θ, resulting in that the total drag decreases along the θ.

Figs. 5(a), 5(b) and 5(c) show the time-averaged streamlines in the spanwise-normal plane at the maximum dimple-imprinted depth for CASE1, CASE3 and CASE5, repectively.

In general, the flow structures near the General Dimple and Riblet-mounted Dimple are similar as follows. After the flow separated at the rim located in the upstream direction of the dimple, it is swallowed inside the dimple, and then it impinges on the concave surface located in the downstream portion inside the dimple. Finally, the flow is ejected from the dimple through the downstream rim of the dimple.

goodness factor as a function of θ, respectively. In the range of θ from $0°$ to $30°$, the variation of the volume and area goodness factors are minute. However, both two factors rapidly increase as θ increases from $30°$ to $60°$. It is certified by the results of the volume and area goodness factors that the thermo-aerodynamic performance is enhanced by the Riblet-mounted Dimples with the riblet angle larger than $30°$.

Characteristics of the drag and heat transfer

However, the effect of the riblet inside dimple on the flow can be identified by the careful observation of Figs. 5(a-c). Namely, as θ increases, the reattachment of flow occurs early, resulting in that the reattachment location moves toward the upstream portion of the dimple and simultaneously the recirculation zone becomes smaller.

Figs. 6 (a) and 6(b) show the distribution of the time-averaged local Nusselt number at the bottom surface of CASE1 and CASE5, respectively. As expected, the temperature gradient between the surface and adjacent fluid becomes smaller with increasing recirculation region preventing the direct contact of flow to the surface. As above shown in Figs. 5, since the recirculation region decreases with increasing θ, the temperature gradient becomes sharp over the wider region.

CONCLUSIONS

Direct numerical simulations were conducted in order to reveal the mechanisms of the heat transfer enhancement and the reduction of the pressure drop caused by the new surface shape proposed in the present study. The quantity information as the characteristics of flow and thermal fields such as the Nusselt number, Stanton number, Fanning friction factor, volume goodness factor and area goodness factor has been presented in detail. In the present study, the structural features of the Riblet-mounted Dimple for the enhancement of the thermo-aerodynamic performance are summarized as below.

(1) At $\theta = 60°$, the ratios of drag reduction and Nusselt number augmentation are –22.86% and 7.05%, respectively.
(2) The pressure drop is reduced by the installation of the riblet inside dimple.
(3) The heat transfer is enhanced by the Riblet-mounted Dimples with the riblet angle larger than $45°$.
(4) The thermo-aerodynamic performance is enhanced by the Riblet-mounted Dimples with the riblet angle larger than $30°$.

Further studies should be conducted in order to obtain the optimized design parameters of the Riblet-mounted Dimple shape and investigate the thermo-aerodynamic performance for higher Reynolds numbers.

ACKNOWLEDGEMENTS

REFERENCES

Afanasyev, V. N., Chudnovsky, Y. P., Leontiev, A. I. and Roganov, P. S., 1993, "Turbulent flow friction and heat transfer characteristics for spherical cavities on a flat plate", *Experimental Thermal and Fluid Science*, Vol. 7, pp. 1-8.

Elyyan, M. A., Rozati, A. and Tafti, D. K., 2008, "Investigation of dimpled fns for heat transfer enhancement in compact heat exchanger", *International Journal of Heat and Mass Transfer*, Vol. 51, pp. 2950-2966.

Kim, J., Moin, P. and Moser, R., 1987, "Turbulent statistics in fully developed channel flow at low Reynolds number", *Journal of Fluid Mechanics*, Vol. 177, pp. 133-166.

Ligrani, P. M., Harrison, J. L., Mahmmod, G. I. and Hill, M. L., 2001, "Flow structure due to dimple depressions on a channel surface", *Physics of Fluids*, Vol. 13, pp. 3442-3451.

Mahmood, G. I. and Ligrani, P. M., 2002, "Heat transfer in a dimpled channel: combined influences of aspect ratio, temperature, Reynolds number, and flow structure", *International Journal of Heat and Mass Transfer*, Vol. 45, pp. 2011-2020.

Moon, H. K., O'Connell, T. and Glezer, B., 2000, "Channel height effect on heat transfer and friction in a dimpled passage", *Journal of Engineering for Gas Turbines and Power*, Vol. 122, pp. 307-313.

Shah, R. K. and London, A. L., 1978, "Laminar flow forced convection in ducts", *Academic Press, Inc. New York.*

Wang, Z., Yeo, K. S. and Khoo, B. C., 2006, "DNS of low Reynolds number turbulent flows in dimpled channels", *Journal of Turbulence*, Vol. 7, pp. 1~31.

You, J., Choi, H. and Yoo, J. Y., 2000, "Modified fractional step method of keeping a constant mass flow rate in fully developed channel and pipe flows", *KSME International Journal*, Vol. 14, No. 5, pp. 547-552.